CIRP Journal of Manufacturing Science and Technology 38 (2022) 801–812

Contents lists available at ScienceDirect

CIRP Journal of Manufacturing Science and Technology

journal homepage: www.elsevier.com/locate/cirpj

Production of AA1050/silica fume composite by bobbin tool-friction stir processing: Microstructure, composition and mechanical properties

Mohamed M.Z. Ahmed[a,b,c], Mohamed M. El-Sayed Seleman[a,b], Rana G. Eid[a,d], M.F. Zawrah[e,*]

[a] Department of Metallurgical and Materials Engineering, Faculty of Petroleum and Mining Engineering, Suez University, 43512 Suez, Egypt
[b] Suez and Sinai Metallurgical and Materials Research Center of Scientific Excellence (SSMMR-CSE), Suez University, 43512 Suez, Egypt
[c] Mechanical Engineering Department, College of Engineering at Al Kharj, Prince Sattam Bin Abdulaziz University, Al Kharj 16273, Saudi Arabia
[d] Canal High Institute of Engineering and Technology, 43512 Suez, Egypt
[e] National Research Centre, Refractory, Ceramics and Building Material Department, El Buhouth St., 12622 Dokki, Cairo, Egypt

ARTICLE INFO

Available online xxxx

Keywords:
Bobbin tool
Friction stir processing
Bulk composite
AA1050
Silica fume
Mechanical properties

ABSTRACT

In the present study, bobbin tool friction stir processing (BT-FSP) with a cylindrical pin was utilized to produce bulk processed AA1050 and AA1050/6.5 vol% silica fume (SF) composite at a rotation speed of 600 rpm using two travel speeds of 100 and 200 mm/min. The BT-FSP temperature was measured for both processed materials. Phase composition, relative density, macrostructure, hardness, ultimate tensile strength, and compressive strength were examined for the AA1050 base material, processed AA1050 and AA1050/SF composite. The results showed that the temperature of BT-FSP was increased with SF addition. The addition of fine SF resulted in a small crystallite size compared to the AA1050 BM and the processed AA1050. Moreover, the SF addition to the AA1050 matrix improved mechanical properties in terms of hardness, ultimate tensile strength, and compressive strength compared to AA1050 BM and processed AA1050. The bulk AA1050/6.5 vol% nano SF composite produced at 600 rpm and 200 mm/min showed remarkable enhancements in properties compared to AA1050 parent material; i.e. 50% in hardness, 11% in compressive strength, and 40% in ultimate tensile strength.

Introduction

Metal matrix composites (MMCs) reinforced with submicron (< 1 μm) ceramic particles have recently paid a great of interest and offered significant opportunities as structural materials in many engineering applications as they have enhanced mechanical properties compared to micro composites (MCs) or pure metals. These composites could be produced by using many techniques such as; powder metallurgy [1], casting [2,3], infiltration, and friction stir processing (FSP) [4,5]. FSP is a solid-state thermo-mechanical process used intensively during the last ten years to modify the metal microstructure and produces surface composites. This is based on a conventional tool (CT) which improves the mechanical properties of the processed material with/without the addition of ceramic particles [6]. In FSP, a conventional rotating tool with a pin and one shoulder are plunged into the material of workpiece to stir the material when the shoulder and material sheet is contacted. Bobbin tool (BT) is an innovative tool design used in friction stir welding [7]. The name "bobbin" refers to a double-side friction stirring tool formed from double shoulders and pin, one shoulder is affecting the lower surface of the plate and the other one affecting the upper surface of the plates with the pin between them affecting the full thickness microstructure features and mechanical properties [8]. Recently, many publications are directed to bobbin tool friction stir welding (BT-FSW) [9–11], but there are no studies on producing bulk MMCs utilizing the innovative BT facilities in solid-state processing. Moreover, the FSP using BT has many advantages over processing using CT, as low distortion of processed samples due to uniform heat input, low force is required for fixing the samples, and homogeneous temperature distribution through stir zone [12]. Bobbin tool friction stir processing (BT-FSP) starts by driving the BT into the edge of the workpiece with a slow travel speed until plastic deformation is initiated, followed by increasing travel speed to the required value [7]. The main parameters controlling the stirring process in the FSP are; rotational tool speed, travel speed, tool design, downward force, tilt angle, and the type of material undertaken [13–15]. AA 1050 aluminum alloy has paid special attention in various engineering applications such as aerospace, food containers, automobile, chemical, and petrochemical industries due to its ease of production,

* Corresponding author.
E-mail address: mzawrah@nrcsci.org (M.F. Zawrah).

https://doi.org/10.1016/j.cirpj.2022.07.002
1755-5817/

lightweight, low density, and excellent corrosion resistance. Many researchers studied the effect of FSP parameters and the reinforcement by different ceramic particles; TiO_2 [16], Al_2O_3 [17], SiC [18], and TiC [19] to fabricate aluminum matrix composites. Shamanian et al. [20] studied the effect of rotational speed on the friction stir processed Al-12% Si cast-alloy surface hardness. Their results revealed that all processed specimens were defect-free at different parameters and showed higher hardness up to 3 mm down the surface. Mathur et al. [21] reported on the reinforcement of AA5052 metal matrix by TiO_2 ceramic particle. They found that the best hardness (78 HV) and tensile strength (193 MPa) were achieved at rotation speed 1000 rpm and travel speed 65 mm/min. Hoziefa et al. [4] studied the influence of FSP on the microstructure and mechanical properties of the as-cast AA2024-wt%Al_2O_3 nanocomposite. They found that the application of FSP lead to improving the yield strength by 30% and tensile strength by 71% over the as-cast 2024 alloy matrix. Hemendra et al. [22] modified the surface of AA1050 using CT-FSP to produce AA1050/B_4C surface composite at a rotational speed of 1400 rpm and a travel speed of 25 mm/min. The processed surface layer composite showed higher hardness (45 VHN) than the base material (25VHN). Silica fume (SF) is an amorphous material [23] and has a high content of silica. It is produced as a byproduct during production of silicon metal and ferrosilicon alloys after reduction of quartz by carbon. During this process, fumes are evaporated and oxidized when meet with air then form SF powder. The silica content in SF varies according to the type of alloy being produced. It also contains small amounts of iron oxides, magnesium oxides, and alkali oxides. This solid waste has been utilized in many different applications as concrete, composites, ceramics, geopolymers, and others [23,24]. The utilization of silica fume as reinforcement for production of enhanced bulk composite by the proposed tool is considered as added value, economic and eco-friendly when compared to the synthetic highly cost nano ceramics (silica, titania and alumina, etc.) which have been used as reinforcements. Also, few works have been published about the production of bulk composites using the bobbin tool in presence of waste/pure reinforcements. Therefore, the current study is intended to utilize SF as reinforcement for AA1050 to develop AA1050/SF composite using BT-FSP. The produced composites are subjected for full characterization in terms of physical and mechanical properties.

Materials and experimental methods

Materials

AA1050 aluminum alloy sheets with 8 mm thickness were supplied by Egyptian Aluminum Company, Egypt. The AA1050 sheets were cut into 200 mm length x 90 mm width plates. On the other side, the silica fume was provided by Egyptian Ferro Alloys Company-EFACO, Edfou, Aswan, Egypt.

Preparation of AA1050 aluminum/SF composite by Bobbin tool friction-stir processing (BT-FSP)

Bulk metal matrix composite based on a commercial AA1050 aluminum alloy as a matrix and SF powder as reinforcement was produced in solid-state via a novel technology of bobbin tool friction stir processing (BT-FSP). The BT-FPS technique was performed using Bobbin tool (BT) with a cylindrical pin and concave shoulders as shown in Fig. 1a. The dimensions of BT are presented in Fig. 1b. The tool was machined from H13 cold work tool steel and hardened to 52 HRC.

In order to achieve a homogeneous dispersion of SF in the AA1050 aluminum matrix, machined cylindrical holes measuring 2 mm in diameter and 7 mm in depth were arranged in a zigzag line (Fig. 2) on the surface of AA1050 plates. These holes were filled with

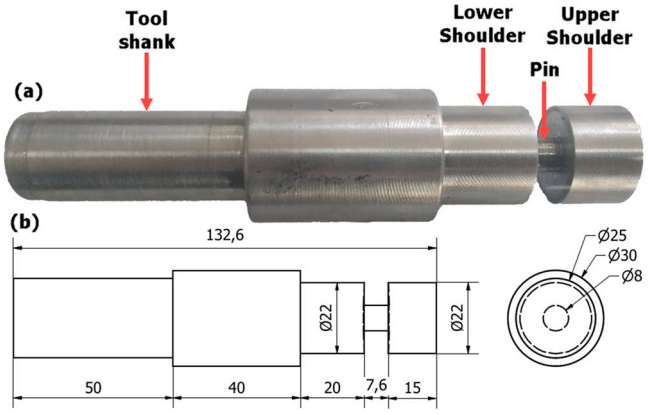

Fig. 1. (a) Photograph and (b) dimensions of bobbin tool (All dimensions in mm).

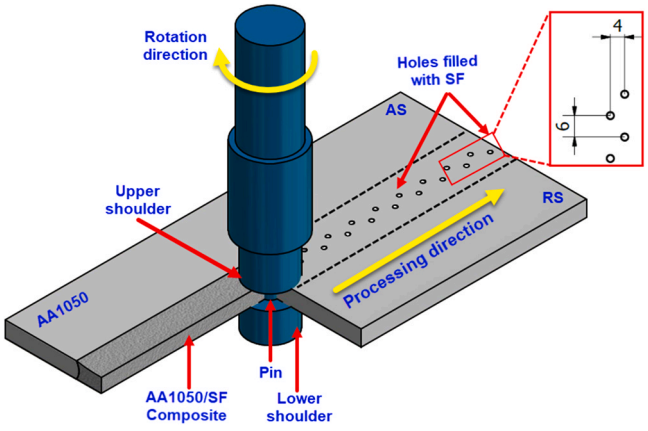

Fig. 2. BT-FSP setup to produce AA1050/SF bulk composite.

submicron SF powder, as given in Fig. 3a, to achieve 6.5 vol% SF in the final produced composites. The BT-FSP was done using FSW machine model EG-FSW-M1 with a specially designed setup fixture system (Fig. 3b). The top and bottom surfaces of produced AA1050/SF composite are shown in Fig. 3c and Fig. 3d, respectively. Different composites were produced at a constant rotation speed of 600 rpm and two processing travel speeds of 100 and 200 mm/min. The tilt angle of the BT axis was kept at zero to prevent sputtering of SF powders from the holes during the stirring process. Full penetration of the tool through the whole thickness of the plate was performed during the BT-FSP process. These processing parameters in terms of rotational speed, travel speeds, tool design, and the tilt angle were selected based on our lab experience and previous studies performed on BT friction stir welding of AA1050 aluminum alloy [7]. For comparison purposes, AA1050 aluminum plates were BT friction stir processed at the same parameters without SF addition.

Characterization of as-received SF and produced composites

The chemical composition of as-received silica fume was analyzed by X-ray fluorescence (XRF- type Bruker S4 with Rh source and 2.2 kW power).

The BT-FSP temperature distribution along the processed and the bulk composite materials was measured at the processing surface behind the BT using an infrared thermometer type; Quicktemp 860-T3, Testo Company - Berlin, Germany. The produced AA1050/SF composites and the processed AA1050 aluminum alloy samples without SF were cut perpendicular to the processing direction (Fig. 4), ground, and polished up to 0.05 µm surface finish for macrostructure investigation. Specimens of the as-received AA1050

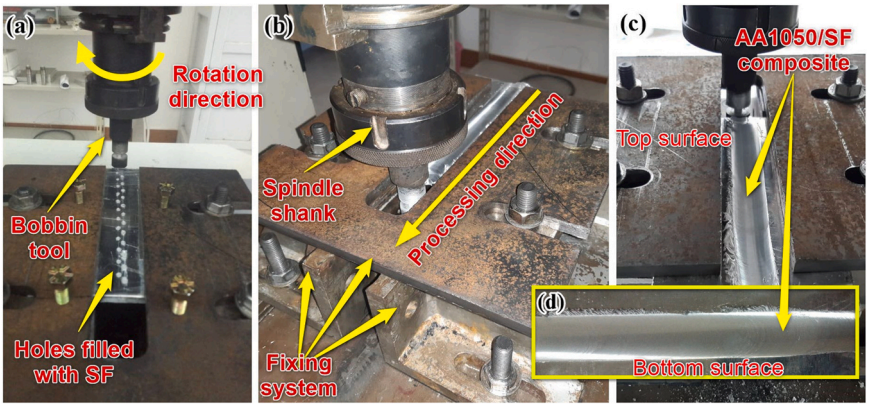

Fig. 3. BT-FSP lab facilities to produce AA1050/SF bulk composite. (a) beginning of the process, (b) end of the process, and (c) and (d) top and bottom surfaces of the produced composite, respectively.

aluminum alloy were prepared at the same condition for comparison purposes. X-ray diffraction (XRD) was utilized to investigate the qualitative phase composition of the as-received SF powder, as-received AA1050 alloy, the processed AA1050 alloy, and the produced composites. X-ray diffraction equipment model Siemens-D5000 with Cu-Kα radiation (wavelength λ = 0.15406 nm) at 40 kV and 30 mA in the 2θ-range from 10° to 100° and step size 0.03° was used. The physical properties in terms of bulk density of selected samples (as-received material, the processed material and the produced composite) were measured based on Archimedes' principle using ethylene glycol (1.11 g/cm^3) as measuring medium. Vickers hardness of all cross-sectional for produced composites, the processed specimens and the base material was measured using a Vickers hardness tester machine (HWDV-75, TTS Unlimited, Osaka, Japan) with a load of 0.3 kg and a dwell time of 15 s. The composite and processed aluminum alloy samples were cut from the processing pass for hardness testing and all other experiments, as given in Fig. 4. The hardness maps were conducted by collecting seven vertical and five horizontal lines as presented i**n** Fig. 5. The tensile and compression tests are conducted at room temperature on a universal testing machine (Universal Testing Machine, WDW-300D Testing Machine, 30-ton, Guangdong, China). The fracture surfaces of the tensile failed specimens were examined using a scanning electron microscope (SEM, Thermo-Scientific, Quattro S, USA) attached with EDAX unit.

Results and discussion

In this section, the results obtained after characterization of starting materials and developed AA1050/SF composites are presented and discussed.

Characteristics of starting materials

Table 1 illustrates the chemical composition of the as-received AA1050 sheet. It is composed mainly of Al (99.5%) with trace amounts of Fe, Si, Ti, Cu, Zn, Mg, Cr and Mn. On the other hand, the chemical composition of the as-received silica fume is illustrated in Table 2. It is comprised mainly of SiO_2 (94%) with some impurities such as Fe_2O_3, Al_2O_3, MgO, and other traces oxides.

Fig. 6 shows XRD patterns of aluminum base materials and silica fume as well as photograph and SEM image of the silica fume powder. The XRD pattern of aluminum (Fig. 6a) exhibits all typical peaks of aluminum while the XRD pattern of silica fume indicates its amorphous character; only broad low intensity peak at 2-theta equal 21–22° characterizing of amorphous silica is detected. The photograph of the as-received silica fume is appeared in Fig. 6c. It is nearly gray in color and consists of very fine particles. The SEM image of silica fume is shown in Fig. 6d. It is indicated that the particles are homogenous in shape (spherical) and heterogeneous in size; the sizes are ranged between 40 nm and 0.4 μm. Some particles are agglomerated and others are relatively dispersed.

BT-FSP thermal cycles of processed materials

The thermal cycles in the stir zone of processed AA1050 and AA1050/SF processed at a constant rotational speed of 600 rpm and travel processing speed of 100 and 200 mm/min were recorded and shown in Fig. 7. It can be observed that the behavior of thermal cycle curves obtained for the processed AA1050 alloy and AA1050/SF composites at the same applied processing parameters is similar with a remarkable difference in the measured peak temperature at

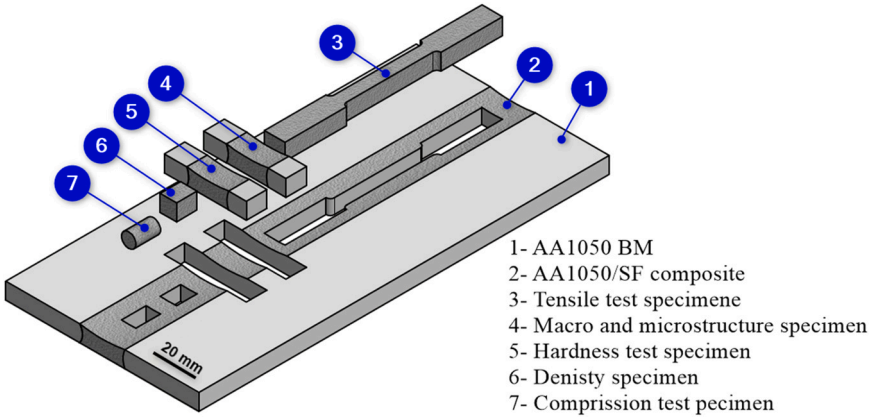

Fig. 4. Schematic drawing shows the location of cutting test specimens for the processed AA1050 and the composite materials.

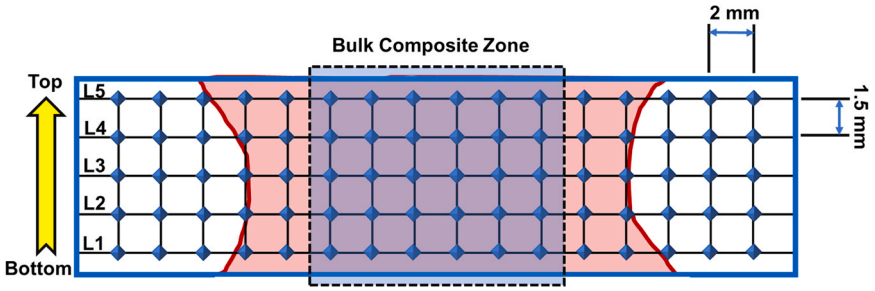

Fig. 5. Schematic drawing of the indentation locations to perform hardness maps.

Table 1
Chemical composition of AA1050 used plates (wt%).

Al	Fe	Si	Ti	Cu	Zn	Mg	Cr	Mn
99.5	0.257	0.0889	0.0139	0.0031	0.0019	0.0030	0.0012	0.0002

Table 2
Chemical analysis of silica fume (wt%).

SiO_2	Fe_2O_3	Al_2O_3	MgO	SO_3	CaO	Na_2O	K_2O	LOI[a]
94.00	2.21	0.79	1.12	0.10	0.48	0.04	0.01	1.25

[a] Loss on Ignition (900 °C, 1 h).

each processing travel speed. The BT-FSP is divided into three steps which are reflected on the thermal cycle and measured temperatures. Firstly, the BT is inserted into the processing zone centerline of the clamped AA1050 plate or its composite with applying the rotation processing speed of 600 rpm and slow processing travel speed of 30 mm/min. In this stage, the materials are heated to a temperature capable of stirring. Secondly, the holding time is adjusted

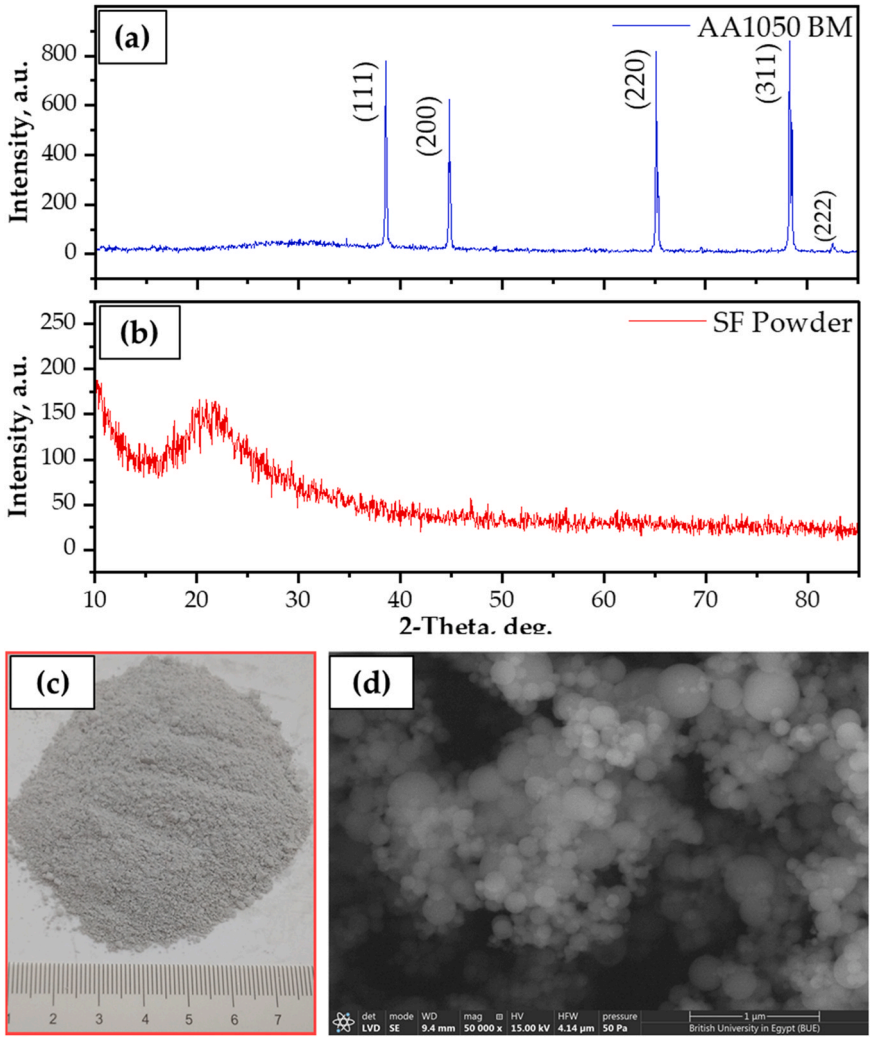

Fig. 6. XRD patterns of AA1050 matrix (a) and silica fume powder (B), as well as photograph (c) and SEM image (d) of as received silica fume.

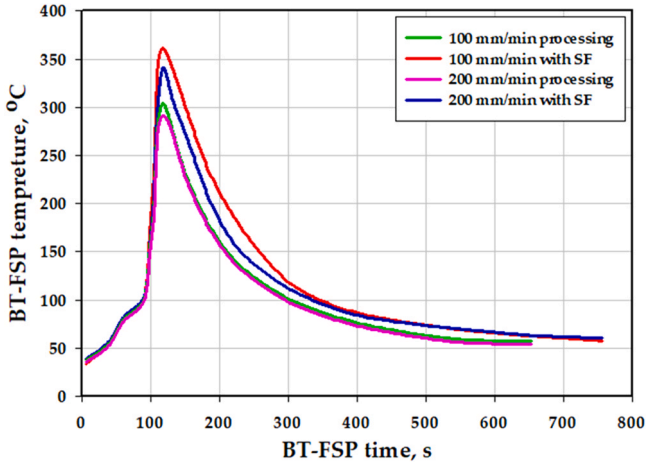

Fig. 7. Temperature histogram during the BT-FSP of processed AA1050 in the presence and absence of SF at a rotation speed of 600 rpm and different travel speeds of 100 and 200 mm/min.

for 20 s to preheat the processed plates. Thirdly, the 100 or 200 mm/min processing travel speed is adopted to start achieving processing of materials passes. In this stage, the temperature of is increased gradually to reach a peak temperature. Finally, the processed AA1050 and its composites are gradually air-cooled with a loss in temperature.

The average temperature values during the BT-FSP of AA1050 and its composite with SF as a function of processing travel speeds 100 and 200 mm/min at a constant rotation speed of 600 rpm is recorded and plotted in Fig. 8. It can be seen that for all processed AA1050 and its composite, as the processing travel speed increases, the maximum temperature decreases. This trend agrees well with that reported in the literatures [7]. It is also noted from Fig. 8 that the presence of SF ceramic particles increases the temperature in the stir zone compared to the processed AA1050 alone. The temperature in the stir zone of AA1050/SF composite is increased by around 20% and 18% at processing speeds of 100 and 200 mm/min, respectively. This is attributed to the presence of harder SF ceramic particles which hinder the stirring process of the deformed material around the pin, then increase the friction between the stirred materials (AA1050 and SF powder) and the tool that causes rising in temperature. These thermal cycles and temperatures experienced upon the BT-FSP are directly reflected on the macro and microstructural features of the processed materials as discussed in the next sections.

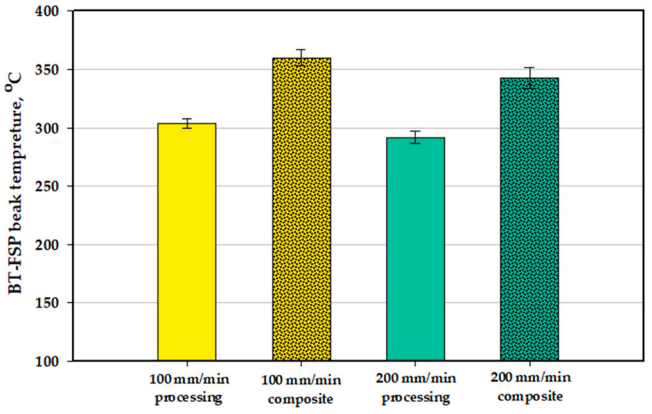

Fig. 8. Effect of SF addition on the peak temperature in the stir zone of the processed AA1050 at a rotation speed of 600 rpm and different travel speeds of 100 and 200 mm/min.

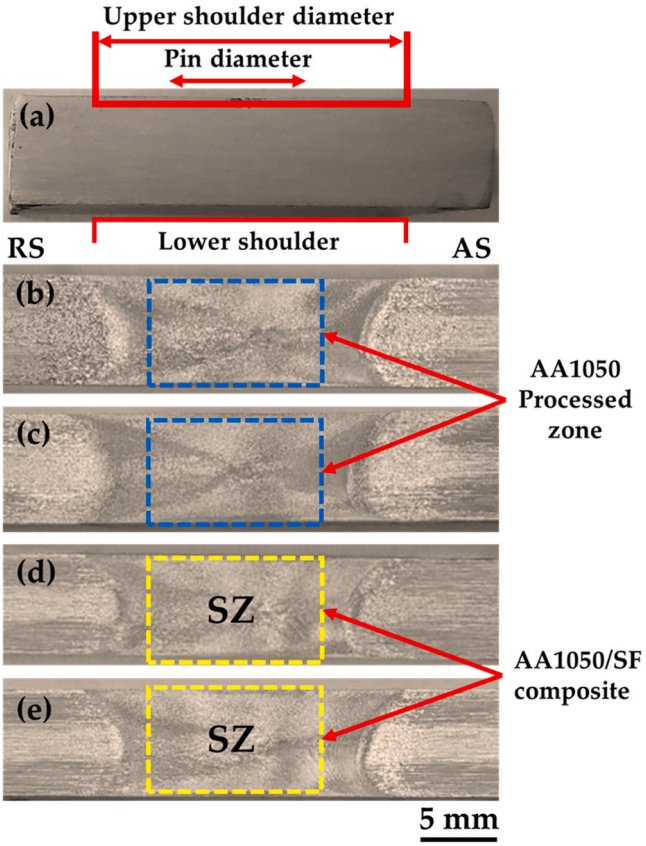

Fig. 9. Cross-section macrostructures of (a) BM, (b) and (d) represent the processed AA1050, and AA105-/SF produced at 600 rpm, and 100 mm/min, respectively, (c) and (e) show the processed AA1050 and AA105-/SF produced at 600 rpm and 200 mm/min, respectively.

Macrostructure of processed materials

The macrostructure on the cross-section of the FSPed specimens is an important feature to evaluate the internal quality of the processed zone and to find out any macro defects that cannot be detected visually. Fig. 9 represents the cross-sectional macrostructures of the BT-FSPed AA1050 and AA1050/SF composite as compared to unprocessed AA1050 (BM), under the aforementioned conditions. Defect-free specimens are obtained for all processed AA1050 and AA1050/SF composite, as shown in Fig. 9a-e. It is also noticed that the cross-sectional shape of the stir zone of BT-FSPed specimens is an hourglass shape. This phenomenon is commonly observed feature in bobbin tool friction stir processed (BT-FSPed). Unlike the conventional tool friction stir processing (CT-FSP), the stir zone in the BT-FSP has an hourglass shape. This is ascribed to the contact and friction heat produced from the upper and lower shoulders [25,26]. The cross-section area of BT-FSP stir zone for processed materials was measured through the thickness of the produced specimens and plotted as given in Fig. 10. It is appeared that the stirring zone area of AA1050 processed and AA1050/SF composite samples are slightly decreased with increasing the travel speed from 100 to 200 mm/min. The stir zone (dynamically recrystallized zone) is the region of sever plastic deformation for material during stirring process in the FSW or the FSP. It roughly relates to the location of the pin. The increase in temperature will allow more softening of the material around the tool, enabling a larger area to be sheared and stirred around the tool. Thus, it can be said that the stirring area increases with an increase in the processing peak temperature of the stir zone, as shown in Fig. 8. This finding is agreed well with that reported by Barbini et al. [27]. They found that the width of the stir

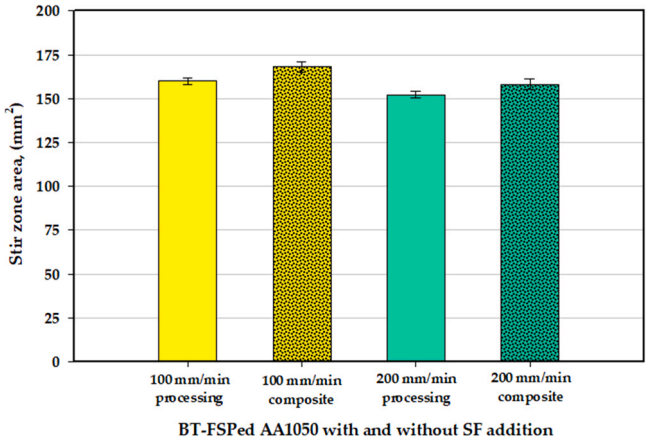

Fig. 10. Stir zone area as a function of processing parameters with and without SF addition.

zones increases with increasing in the heat input. It is worth mentioning that the AA1050/SF composites show a slight increase in the stir zone area in the presence of SF compared to the AA1050 processed specimens without SF addition [25,28] Thus, the applied FSP conditions have resulted in high quality thickness of AA1050/SF composite.

Phase composition and physical properties of processed materials

XRD patterns of AA1050 and AA1050/SF composite processed at different conditions are presented in Fig. 11. All patterns of processed materials exhibit the typical peaks of AA1050 in 2θ range from 35 to 84° [29]. These peaks have index planes of (111), (200), (220), (311), and (222) at 2θ equal 38, 45, 65, 78, and 73°, respectively. It can be observed that by applying the thermo-mechanical process (BT-FSP), there is no considerable change in peak location but the peaks become broad slightly with increasing the travel speed. For the processed AA1050/SF composites (Fig. 11a&b), characteristic hump of amorphous silica at the 2θ from 15 to 30° is detected in both composites prepared using different travel speeds of 100 and 200 mm/min. The presence of this hump in both composites indicate the success of BT-FSP to disperse the amorphous SF in AA1050 Al alloy in solid-state to fabricate composites. One of the essential structural parameters of material is crystallite size. It can be extracted from XRD results, and it is related to the diffraction peak broadening. A slight peak broadening is noted, particularly for the smallest values of crystallite sizes. The crystallite size is reduced from 150 nm for AA1050 BM to be around 90 for the processed materials at 100 mm/min and 81 nm for the processed materials at 200 mm/min (Fig. 12), indicating grain refining. Similar results were obtained by Rahmatabadi et al. [30] as they correlated the grain refining of AA1050 subjected to seven passes accumulative roll bonding to the reduction of crystallite size compared to the annealed AA1050 BM. Several works have been reported on the grain refining of microstructure for composites processed by FSP due to the dynamic recrystallization [31]. In the present study, the crystallite size of the produced composites reached the values of 63 and 49 nm for the composites produced at 100 and 200 mm/min, respectively. This reduction refers to the grain refining of the produced composites due to the double action of dynamic recrystallization and the presence of submicron SF mechanisms.

It is well known that the addition of SF into AA1050 matrix can affect the density of produced composites. Fig. 13 depicts the relative density of unprocessed AA1050 and BT-FSPed AA1050 & AA1050/6.5 vol% SF composite processed at travel speeds of 100 and 200 mm/min. As seen in Fig. 13, a slight increase in the relative density of

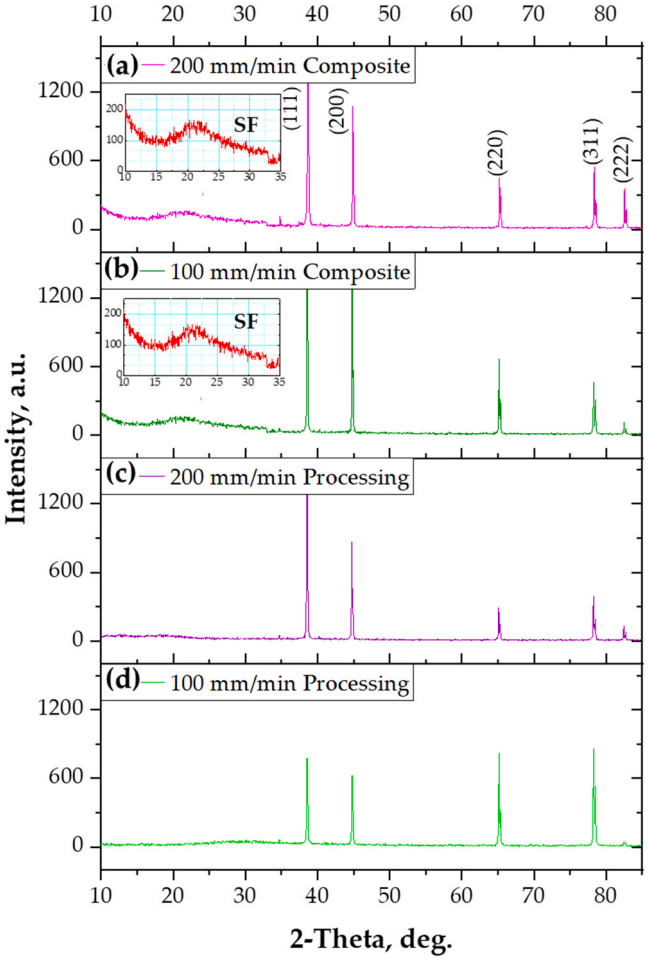

Fig. 11. XRD patterns of the AA1050/6.5 vol% nano SF composites produced at (a) 200 mm/min (b) 100 mm/min and the processed AA1050 material produced at (c) 200 mm/min and (d) 100 mm/min.

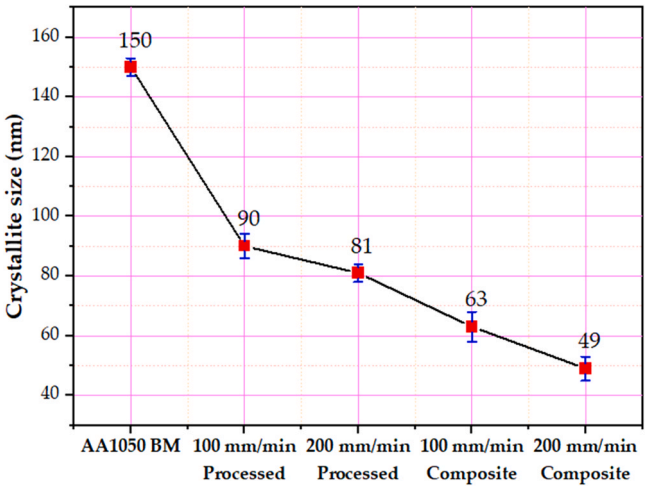

Fig. 12. Crystallite size of the BM, AA1050 processed materials and AA1050/6.5 vol% nano SF composites.

AA1050 processed specimens over the as-received AA1050 material. Also, a slight increase in the relative density is detected for the produced A1050/SF composites compared to the BM and the processed AA1050 samples. This increase may be attributed to the stirring action and the addition of submicron SF which densifies the as-received material. Kumar et al. [32] reported on the improvement

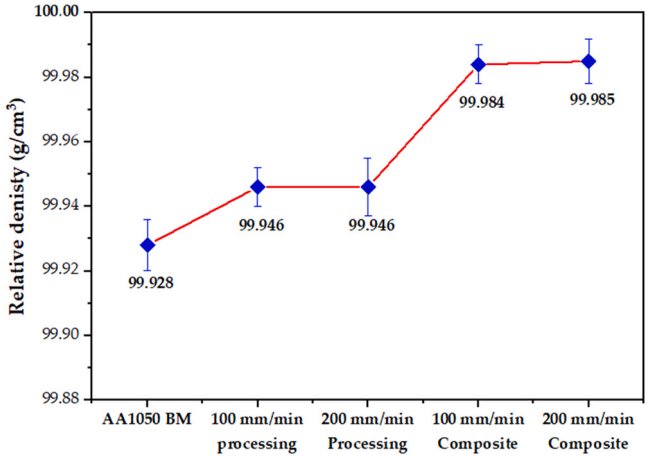

Fig. 13. Effect of BT-FSP and SF addition on the relative density of the as-received AA1050.

of density for AA7075 after addition of SiC. El-Sayed Seleman et al. [33] also reported on the enhancement of relative density for the hot extruded AA6016 with the addition of graphite from 5 to 10 vol%.

Mechanical properties of processed materials

Hardness of processed materials

Hardness measurement is considered one of the main mechanical properties of produced composite materials. It can be affected by the matrix features, reinforcement properties (type and size), and the applied processing parameters. In the current study, the effect of processing parameters (travel speed and the submicron SF addition) on the hardness measurements was performed and compared with that of BM. Fig. 14 shows Vickers hardness maps obtained along the

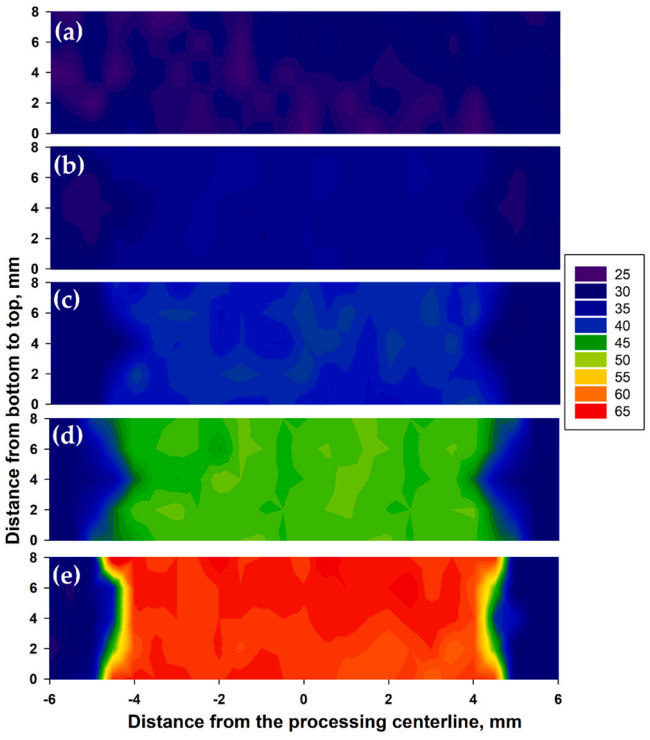

Fig. 14. Hardness maps of (a) AA1050 Bm, AA1050 processed samples produced at (b) 100 mm/min and (c) 200 mm/min, and AA1050/SF composite produced at (d) 100 mm/min and (e) 200 mm/min.

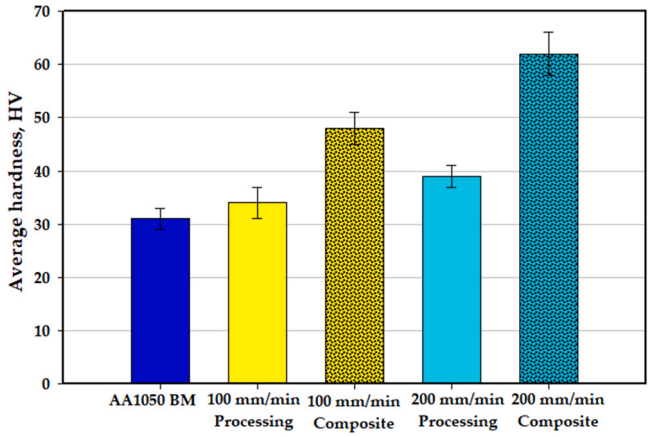

Fig. 15. Average hardness of the AA1050 BM, AA0150 processed samples and the AA1050/6.5 vol% nano SF composites.

transverse cross-sections of the BM (Fig. 14-a) and the processed AA1050 at 600 rpm and two travel speeds of 100 mm/min (Fig. 14-b) and 200 mm/min (Fig. 14-c) compared with the AA1050/SF composites processed at the same conditions (Fig. 14 d and e). Generally, the hardness profile of AA1050 BM (Fig. 14-a) indicates the typical hardness profile for the strain hardened aluminum alloy with the average hardness value of 31 ± 2 HV. This hardness value is mainly affected by the thermo mechanical experience and the submicron SF addition. At a constant rotation speed of 600 rpm, a higher travel speed of 200 mm/min has increased the hardness level in the processed zone by 25% compared with the hardness measurements of the BM. On the other hand, the hardness obtained at 100 mm/min is only increased by 10% over the BM, as shown in Fig. 15. It was reported that the enhancement in hardness in the FSP zone of the aluminum alloys is related to the grain refining due to dynamic recrystallization [34,35]. This grain refining is governed by the heat input produced during the friction stirring process. At a constant rotation speed, the heat input increases with the decreasing of travel speed. Thus, the heat input produced at 100 mm/min is higher than that generated by 200 mm/min travel speed. If the heat input exceeds the optimum value of dynamic recrystallization, the newly formed fine grain size grows, resulting in a drop in hardness. Ahmed et al. [7] mentioned that the optimum heat input to grain refine AA1050 microstructure using bobbin tool friction stir welding at a rotation speed of 600 rpm is 200 mm/min travel speed. This finding confirms the increased hardness of the processed AA1050 at 200 mm/min over both the processed material at 100 mm/min and the BM. The hardness map profiles of AA1050/SF composite processed at 100 and 200 mm/min are shown in Fig. 14-d and Fig. 14-e, respectively. It can be noted that an increase in hardness is achieved by adding 6.5 vol% submicron SF particles compared with processed AA1050 and BM. The hardness reached about 48 and 62 HV for AA1050/SF composite produced at 100 and 200 mm/min, respectively, as shown in Fig. 15. It can be seen that the addition of SF particles exhibit a pronounced effect on the hardness of produced composites. These ceramic particles have high hardness than the AA1050 BM; therefore, it is expected that the dispersing of 6.5 vol% SF in the AA1050 matrix exhibits high levels of hardness for the produced composites. If they are agglomerated, they can act as preferred nucleation sites via particle stimulated nucleation (PSN) mechanism to form new grains during dynamic recrystallization [4,33]. The presence of fine-ceramic particles may hinder grain coarsening by impeding the boundaries and resulting in more refined grains [36].

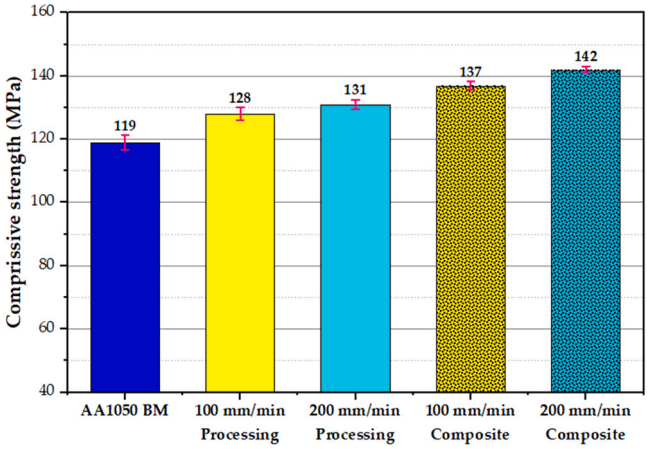

Fig. 16. Compressive strength of the AA1050 BM, AA0150 processed samples and the AA1050/6.5 vol% nano SF composites.

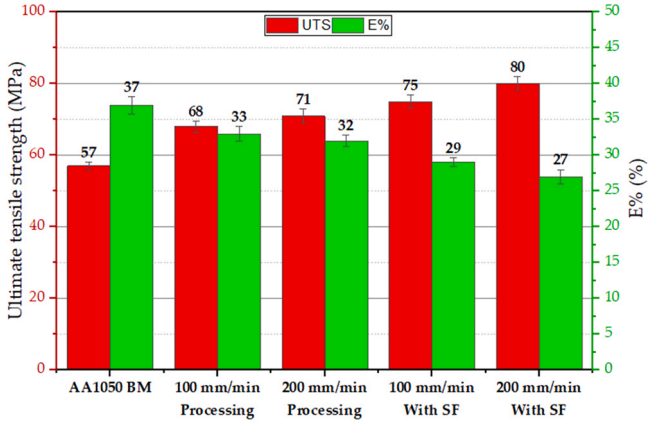

Fig. 17. Ultimate tensile strength and elongation of the AA1050 BM, AA0150 processed samples and the AA1050/6.5 vol% nano SF composites.

Compressive and tensile strengths of processed materials

The compressive strengths at 30% strain of the as-received AA1050, processed AA1050, and AA1050/SF composite produced at 100 and 200 mm/min travel speeds are presented in Fig. 16. It can be noted that a slight increase in compressive strength for both the processed AA1050 specimens without SF addition compared to AA1050 BM by around 8.5%. Whereas a remarkable enhancement in compressive strength is detected for the composites produced at 100 and 200 mm/min by 15% and 19%, respectively, as compared to the as-revived AA1050. The improvement in compressive strength of the processed AA1050 and AA1050/SF composites compared to BM is ascribed to the grain refining achieved by the BT-FSP. In addition, the enhancement of compressive strength of composites over the processed specimens has also been ascribed to the presence of fine SF ceramic particles. The introduction of SF ceramic fine particles to the aluminum matrix increases the grain refining and hinders the dislocation mobility besides the strong multidirectional thermal stress due to the difference of thermal expansion coefficient between AA1050 and SF and the higher compressive strength of the SF ceramic phase compared to the AA1050 BM. Similar findings reported significant enhancements in compressive strength for the many aluminum based composites reinforced with different ceramic particles; Al/SiC [37,38], Al/Si_3N_4 [39], Al/Al_2O_3 [38,40].

During BT-FSP, material suffers from severe plastic deformation combined with sufficient high temperature to achieve dynamic recrystallization (DRX), resulting in grain refining compared to the parent material [18]. In case of BT-FSPed AA1050, the governing factor to keep recrystallizing grain refining is the heat input. However, in case of BT-FSPed AA1050/SF composite, the circumstance is changed. In the friction stir processing of nearly pure aluminum, the formed newly fine grain size is so sensitive to further increase in temperature, and the higher temperature promotes grain boundary migration [16,41]. While in the aluminum-based composites reinforced with ceramic particles, the reinforcing phase acts as a barrier to grain growth by hindering the boundary migration. This phenomenon is recognized as the pinning effect [42]. Furthermore, the reinforcing nanoparticles could break up the initial grains during the stirring process, increasing the nucleation sites for recrystallization. The more the primary recrystallized grains, the finer the obtained microstructure [42]. The inclusion of nano reinforcing ceramic particles not only increases the number of grain boundaries through grain size refinement, which results in increased strength by inhibiting dislocation mobility but also increases the dislocation density [36,43]. As a result, it's likely that this aspect contributed to the ultimate tensile strength's improvement. The two most important aspects that influenced the mechanical characteristics of the stirred zone material are grain refinement and dislocation strengthening, while the decrease in dislocation density also caused the elongation reduction. Grain refinement increases grain boundary volume, preventing dislocation movement during tensile testing or, more particularly, plastic deformation [44]. Fig. 17 shows the **u**ltimate tensile strength and elongation of AA1050 BM, AA0150 and the AA1050/6.5 vol% nano SF composites. It can be seen that the AA1050/SF nano composites produced via BT-FSP at 600 rpm using travel speeds of 100 and 200 mm/min show higher ultimate tensile strength and lower elongation compared to the processed AA1050 and the as-received AA1050 BM (Fig. 17). This is attributed to grain refinement and strengthening associated with the addition of fine SF powder to the aluminum matrix. Depending on the size of SF particles, the dislocations can either shear or bow around the particles, resulting in two circumstances. Firstly, if there are tiny nanoparticles, dislocations pile-up till shearing of the particles, resulting in strengthening [45]. Secondly, the development of loops will occur for large-sized nanoparticles, which is another reason for material strengthening [46]. It can be concluded that the BT-FSP parameters of 600 rpm and 200 mm/min travel speed produces AA1050/6.5% SF composite materials having the highest ultimate tensile strength of 80 MPa compared to the other processed specimens and BM.

Microstructure of fracture surfaces after tensile strength measurement

The microstructure of fracture surfaces after tensile test for processed materials are shown Figs. 18–20. They exhibits SEM images at different magnifications for AA1050 BM (Fig. 18), AA1050 (Fig. 19) and AA1050/6.5 vol% SF composite (Fig. 13) processed at 200 mm/min travel speed. The SEM images of AA1050 BM show large dimples with tearing edges and serrations indicating ductile fracture (Fig. 18). Moreover, micro-cracks are detected on the fracture surface (Fig. 18**-c**). The fracture surface of the processed AA1050 contains equiaxed shallow and deep dimples that are smaller than observed for the BM (Fig. 19) indicating grain refining due to dynamic recrystallization combined with the processing at 600 rpm and 200 mm/min. This result is confirmed with the crystallite size results (Fig. 12). Since the nucleation of micro-voids, the dimples in the AA1050 BM are deeper than those in the processed sample, and subsequent coalescence is impacted by the shear stress component, resulting in elongated dimples in the direction of the shear stresses. After addition of fine SF, the fracture surface is dominated by equiaxed, uniform, and homogeneous smaller dimples with thinner edges (Fig. 20 a-c) compared to the AA1050 BM and AA1050

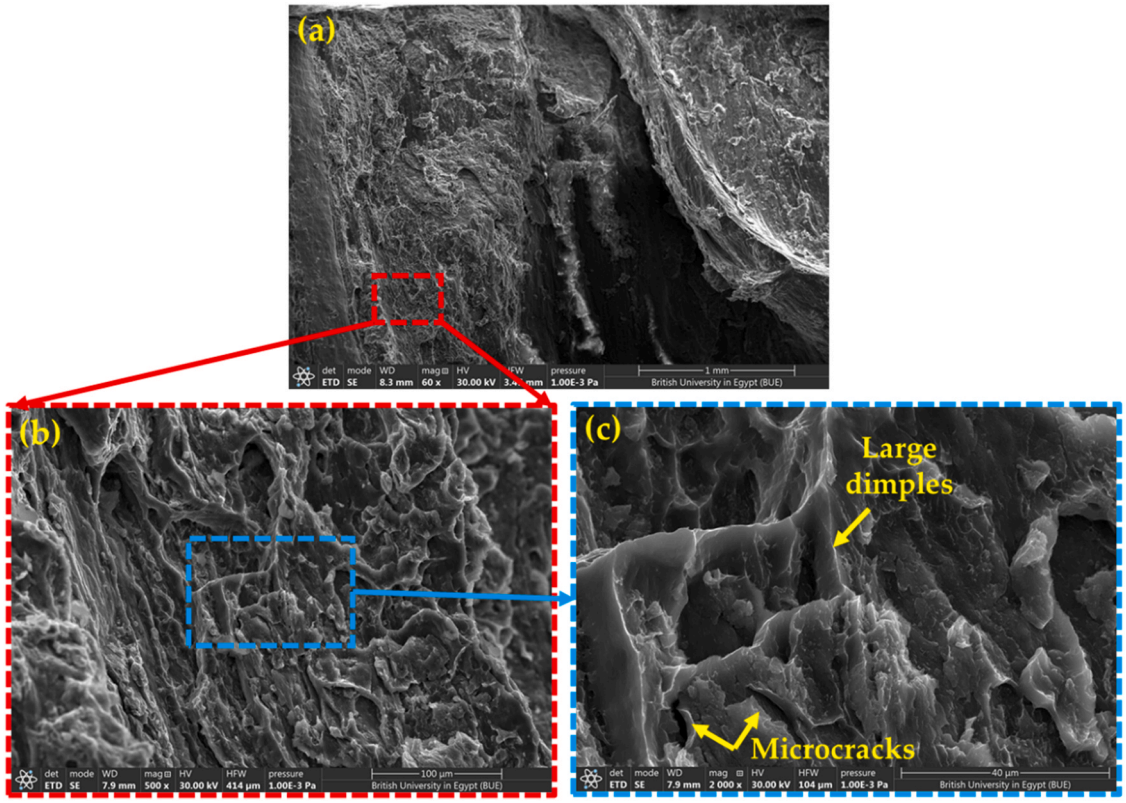

Fig. 18. SEM images at different magnifications of fracture surface for AA1050 BM (a) 60x, (b) 500x and (c) 2000x.

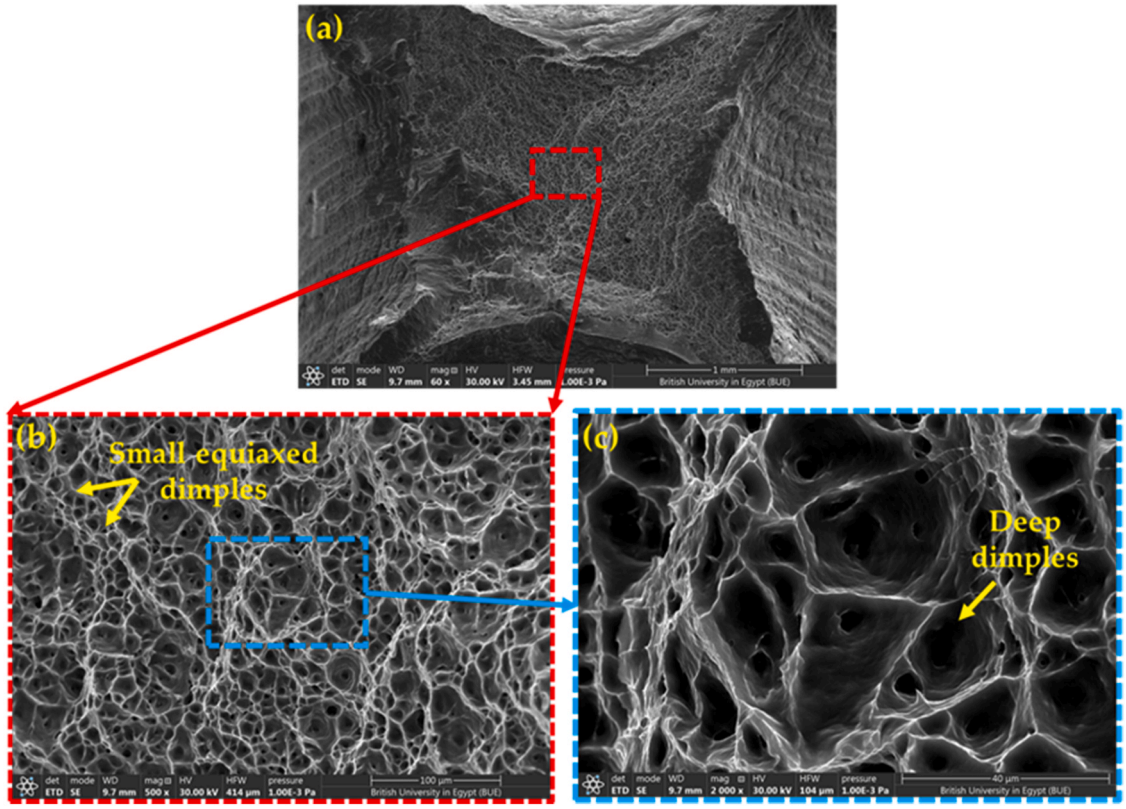

Fig. 19. SEM images at different magnifications of fracture surface for AA1050 processed samples produced at 200 mm/min and 600 rpm (a) 60x, (b) 500x and (c) 2000x.

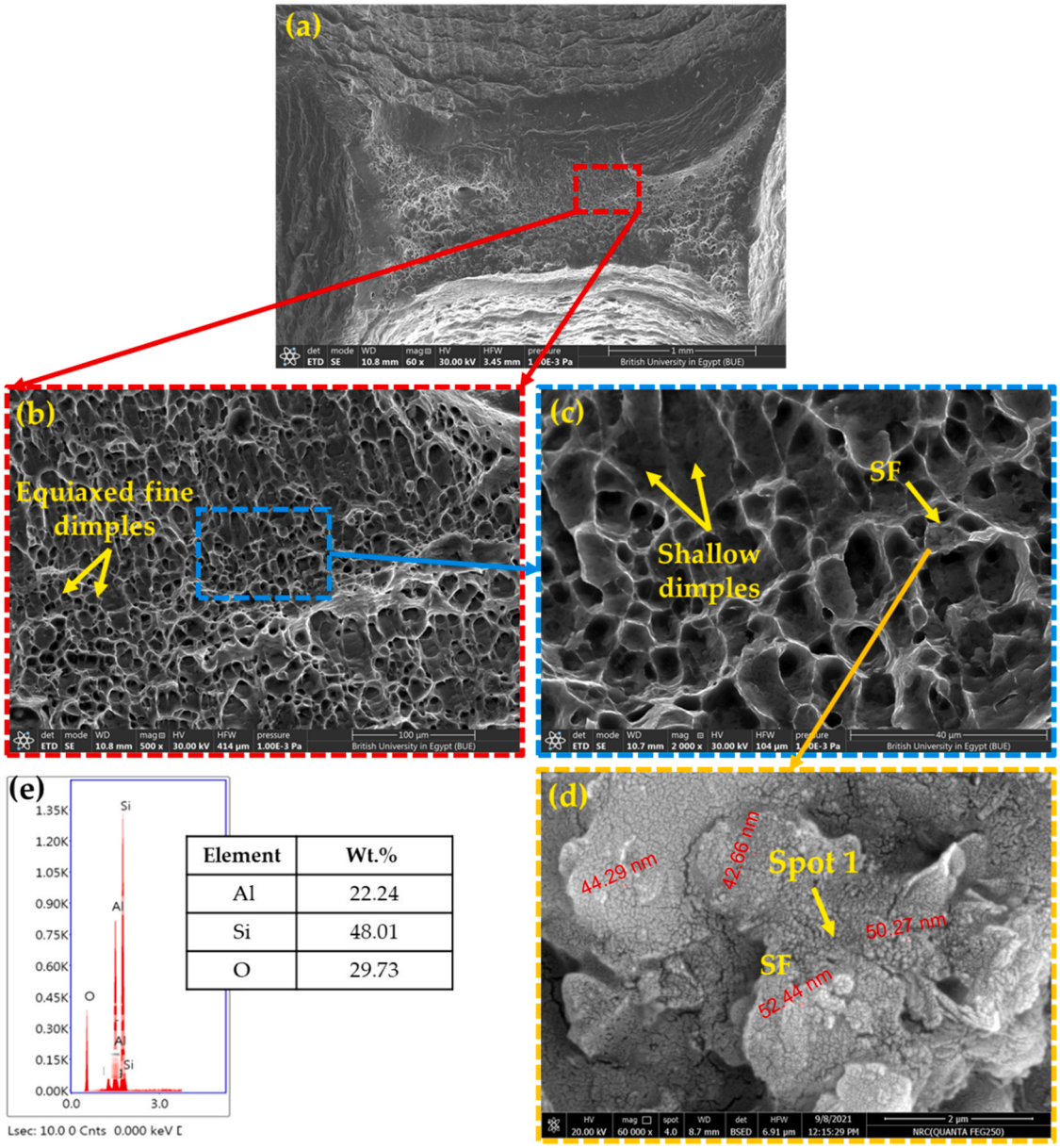

Element	Wt.%
Al	22.24
Si	48.01
O	29.73

Fig. 20. SEM images (different magnifications) of fracture surface and spot analysis for AA1050/6.5 vol% nano SF produced at 200 mm/min and 600 rpm (a) 60x, (b) 500x (c) 2000x, (d) 60,000 x, and (e) spot analysis of point in (d).

processed sample indicating more grain refining. Some dimples filled with nano SF are detected in Fig. 20-d and confirmed by EDS spot analysis given in Fig. 20-c. The filled dimples with SF appear brittle fracture features due to the presence of ceramic phase. Despite this phenomenon, the fracture surface is mainly ductile. The randomly measured SF particles on the fracture surfaces of the produced composite ranged from 42 to 52 nm. This particle size range less than the range of the starting SF particles. In addition, there is no remarked agglomeration of the SF particles through the AA1050 cross-section indicating the efficiency of BT-FSP to disperse the nano-ceramic particles through the AA1050 matrix at the processing parameters of 600 rpm and 200 mm/min processing speed. In general, the dispersion of the nano ceramic particles in the matrix to produced composites (during the FSP) is governed by the processing parameters in terms of travel speed, rotation speed, tool geometry, and number of passes [47,48]. In addition, the particle morphology, size, and volume fraction have a great effect on the dispersion process [33,49].

Conclusions

BT-FSP technique was successfully utilized to produce bulk AA1050 processed and AA1050/6.5 vol% nano SF composite materials at a constant rotation speed of 600 rpm and two travel speeds of 100 and 200 mm/min. The following conclusions could be drawn:

1. Using the proposed technique, processed AA1050 and AA1050/SF composite with 8 mm thickness and 8 mm width along the processing path were produced.
2. The hardness, ultimate tensile strength, and compressive strength of processed AA050 and AA1050/SF composite were increased with increasing travel speed from 100 to 200 mm/min.
3. Among the applied conditions, the processing at 600 rpm and 200 mm/min using the designed bobbin tool is recommended to produce bulk AA1050/6.5 vol% nano SF composite having an average hardness of 62 HV, ultimate tensile strength 80 MPa, and compressive strength of 142 MPa.

4. The addition of 6.5 vol% fine SF to the AA1050 matrix resulted in a small crystallite size compared to the processed AA1050 and as-received AA1050. The AA1050/SF composite produced at 200 mm/min travel speed revealed a smaller crystallite size (49 nm) than the composite sample produced at 100 mm/min (63 nm).
5. The SF addition improved the mechanical properties in terms of hardness, ultimate tensile strength, and compressive strength for AA1050/SF composite compared to AA1050 BM and AA1050 processed samples.

Declaration of Competing Interest

The authors declare that they have no known competing financial interests or personal relationships that could have appeared to influence the work reported in this paper.

References

[1] Singh, H., Singh Brar, G., Kumar, H., Aggarwal, V., 2020, A Review on Metal Matrix Composite for Automobile Applications. Materials Today: Proceedings, 43:320–325. https://doi.org/10.1016/j.matpr.2020.11.670.

[2] Kumar, R., Pradeep, S., Singh, R., Dubey, R., Dwivedi, S.P., 2021, A Critical Review on Different Casting Technique to Develop the Composite Material and its Tribo-mechanical Behaviour. Materials Today: Proceedings, 47:3895–3900. https://doi.org/10.1016/j.matpr.2021.03.551.

[3] Joslin Vijaya, D., Pradeep Kumar, J., Robinson Smart, D.S., 2021, Analysis of Hybrid Aluminium Composite Material Reinforced with Ti and NbC Nanoparticles Processed through Stir Casting. Materials Today: Proceedings, 1–10. https://doi.org/10.1016/j.matpr.2021.05.683.

[4] Hoziefa, W., Toschi, S., Ahmed, M.M.Z., Morri, A., Mahdy, A.A., El-Sayed Seleman, M.M., El-Mahallawi, I., Ceschini, L., Atlam, A., 2016, Influence of Friction Stir Processing on the Microstructure and Mechanical Properties of a Compocast AA2024-Al2O3 Nanocomposite. Materials and Design, 106:273–284. https://doi.org/10.1016/j.matdes.2016.05.114.

[5] Awad, O., Seleman, M., Ahmed, M., Ammar, H., 2018, Production and Characterization of AA7075-Graphite Composite Using Friction Stir Processing. Journal of Petroleum Science and Engineering, 20:101–110. https://doi.org/10.21608/jpme.2018.40652.

[6] Arora, H.S.; Singh, H.; Dhindaw, B.K. Composite fabrication using friction stir processing - A review. In Proceedings of the International Journal of Advanced Manufacturing Technology; 2012; Vol. 61, pp. 1043–1055.

[7] Ahmed, M.M.Z., Habba, M.I.A., El-Sayed Seleman, M.M., Hajlaoui, K., Ataya, S., Latief, F.H., EL-Nikhaily, A.E., 2021, Bobbin Tool Friction Stir Welding of Aluminum Thick Lap Joints: Effect of Process Parameters on Temperature Distribution and Joints' Properties. Materials, 14.

[8] Fuse, K., Badheka, V., 2019, Bobbin Tool Friction Stir Welding: A Review. Science and Technology of Welding and Joining, 24:277–304. https://doi.org/10.1080/13621718.2018.1553655.

[9] Wen, Q., Li, W., Patel, V., Bergmann, L., Klusemann, B., dos Santos, J.F., 2021, Assessing the Bonding Interface Characteristics and Mechanical Properties of Bobbin Tool Friction Stir Welded Dissimilar Aluminum Alloy Joints. Acta Metallurgica Sinica (English Letters), 34:125–134. https://doi.org/10.1007/s40195-020-01101-4.

[10] Li, G.H., Zhou, L., Zhang, H.F., Guo, G.Z., Luo, S.F., Guo, N., 2021, Evolution of Grain Structure, Texture and Mechanical Properties of a Mg–Zn–Zr Alloy in Bobbin Friction Stir Welding. Materials Science and Engineering A, 799. https://doi.org/10.1016/j.msea.2020.140267.

[11] Mardalizadeh, M., Khandaei, M., Safarkhanian, M.A., 2020, Influence of Travel Speed on the Microstructural Evaluation and Mechanical Characteristics of Bobbin Tool Friction Stir-welded Thick AA5456-H112 Plates. Journal of Adhesion Science and Technology, 0:1–20. https://doi.org/10.1080/01694243.2020.1792156.

[12] Goetze, P., Kopyściański, M., Hamilton, C., Dymek, S., 2019, Comparison of Dissimilar Aluminum Alloys Joined by Friction Stir Welding with Conventional and Bobbin Tools. Minerls, Metals and Materials Series, 3–12. https://doi.org/10.1007/978-3-030-05752-7_1.

[13] Huang, Y., Xie, Y., Meng, X., Lv, Z., Cao, J., 2018, Numerical Design of High Depth-to-width Ratio Friction Stir Welding. Journal of Materials Processing Technology, 252:233–241. https://doi.org/10.1016/j.jmatprotec.2017.09.029.

[14] Bhavya Swathi, I., Suvarna Raju, L., Ramulu, P.J., 2020, Surface Development by Reinforcing Nano-composites During Friction Stir Processing – A Review. Journal of Engineering, Design and Technology, 18:653–687. https://doi.org/10.1108/JEDT-02-2019-0043.

[15] Soleymanpour, M., Aval, H.J., Jamaati, R., 2022, Manufacturing of High-toughness Al–Si Alloy by Rolling and Friction Stir Processing: Effect of Traverse Speed. CIRP Journal of Manufacturing Science and Technology, 37:19–36. https://doi.org/10.1016/j.cirpj.2021.12.007.

[16] Mirjavadi, S.S., Alipour, M., Emamian, S., Kord, S., Hamouda, A.M.S., Koppad, P.G., Keshavamurthy, R., 2017, Influence of TiO2 Nanoparticles Incorporation to Friction Stir Welded 5083 Aluminum Alloy on the Microstructure, Mechanical Properties and Wear Resistance. Journal of Alloys and Compounds, 712:795–803. https://doi.org/10.1016/j.jallcom.2017.04.114.

[17] Darzi Bourkhani, R., Eivani, A.R., Nateghi, H.R., Jafarian, H.R., 2020, Effects of Pin Diameter and Number of Cycles on Microstructure and Tensile Properties of Friction Stir Fabricated AA1050-Al2O3 Nanocomposite. Journal of Materials Research and Technology, 9:4506–4517. https://doi.org/10.1016/j.jmrt.2020.02.078.

[18] Srivastava, M., Rathee, S., 2021, A Study on the Effect of Incorporation of SiC Particles during Friction Stir Welding of Al 5059 Alloy. Silicon, 13:2209–2219. https://doi.org/10.1007/s12633-020-00722-9.

[19] Singla, S., Kang, A.S., Sidhu, T.S., 2020, Development and Characterization of WE43/nano-TiC Surface Composite by Friction Stir Processing Technique. Measurement and Control, 53:730–741. https://doi.org/10.1177/0020294019895302.

[20] Shamanian, M., Mostaan, H., Safari, M., Dezfooli, M.S., 2017, Friction-stir Processing of Al-12%Si Alloys: Grain Refinement, Numerical Simulation, Microstructure Evolution, Dry Sliding Wear Performance and Hardness Measurement. Metallurgical Research & Technology, 114. https://doi.org/10.1051/metal/2016066.

[21] Mathur, V., B, S.R.P., Patel G C, M., Shettigar, A.K., 2019, Reinforcement of Titanium Dioxide Nanoparticles in Aluminium Alloy AA 5052 through Friction Stir Process. Adv Mater Process Technol. 5. : 329–337. https://doi.org/10.1080/2374068X.2019.1585072.

[22] Patle, H., Gupta, A., Mahendiran, P., Dumpala, R., 2018, Fabrication of AA1050/B4C Surface Composite by Friction Stir Processing (FSP) and Investigation on Mechanical and Wear Characteristics. IOP Conference Series: Materials Science and Engineering, 402. https://doi.org/10.1088/1757-899X/402/1/012128.

[23] Suri, J., Shaw, L.L., Zawrah, M.F., 2011, Synthesis of Carbon-Free Si3N4/SiC Nanopowders using Silica Fume. Ceramics International, 37:3477–3487. https://doi.org/10.1016/j.ceramint.2011.06.003.

[24] Sadek, H.E.H., Khattab, R.M., Zawrah, M.F., 2016, Preparation of Porous Forsterite Ceramic using Waste Silica Fumes by the Starch Consolidation Method. InterCeram International Ceramic Review, 65:174–178. https://doi.org/10.1007/bf03401166.

[25] Wang, F.F., Li, W.Y., Shen, J., Wen, Q., dos Santos, J.F., 2018, Improving Weld Formability by a Novel Dual-rotation Bobbin Tool Friction Stir Welding. Journal of Materials Science and Technology, 34:135–139. https://doi.org/10.1016/j.jmst.2017.11.001.

[26] Yang, C., Ni, D.R., Xue, P., Xiao, B.L., Wang, W., Wang, K.S., Ma, Z.Y., 2018, A Comparative Research on Bobbin Tool and Conventional Friction Stir Welding of Al-Mg-Si Alloy Plates. Materials Characterization, 145:20–28. https://doi.org/10.1016/j.matchar.2018.08.027.

[27] Barbini, A., Carstensen, J., dos Santos, J.F., 2018, Influence of a Non-rotating Shoulder on Heat Generation, Microstructure and Mechanical Properties of Dissimilar AA2024/AA7050 FSW Joints. Journal of Materials Science and Technology, 34:119–127. https://doi.org/10.1016/j.jmst.2017.10.017.

[28] Wen, Q., Li, W., Patel, V., Gao, Y., Vairis, A., 2020, Investigation on the Effects of Welding Speed on Bobbin Tool Friction Stir Welding of 2219 Aluminum Alloy. Metals and Materials International, (26): 1830–1840. https://doi.org/10.1007/s12540-019-00450-9.

[29] Gashti, S.O., Fattah-alhosseini, A., Mazaheri, Y., Keshavarz, M.K., 2016, Microstructure, Mechanical Properties and Electrochemical Behavior of AA1050 Processed by Accumulative Roll Bonding (ARB). Journal of Alloys and Compounds, 688:44–55. https://doi.org/10.1016/j.jallcom.2016.07.177.

[30] Rahmatabadi, D., Hashemi, R., Mohammadi, B., Shojaee, T., 2017, Experimental Evaluation of the Plane Stress Fracture Toughness for Ultra-fine Grained Aluminum Specimens Prepared by Accumulative Roll Bonding Process. Materials Science and Engineering A, 708:301–310. https://doi.org/10.1016/j.msea.2017.09.085.

[31] Ahmed, M.M.Z., Wynne, B.P., El-Sayed Seleman, M.M., Rainforth, W.M., 2016, A Comparison of Crystallographic Texture and Grain Structure Development in Aluminum Generated by Friction Stir Welding and High Strain Torsion. Materials and Design, 103:259–267. https://doi.org/10.1016/j.matdes.2016.04.056.

[32] Kumar, G.B.V., Rao, C.S.P., Selvaraj, N., Bhagyashekar, M.S., 2010, Studies on Al6061-SiC and Al7075-Al < sub > 2 < /sub > O < sub > 3 < /sub > Metal Matrix Composites. Journal of Minerals and Materials Characterization and Engineering, 09:43–55. https://doi.org/10.4236/jmmce.2010.91004.

[33] El-Sayed Seleman, M.M., Ahmed, M.M.Z., Ataya, S., 2018, Microstructure and Mechanical Properties of Hot Extruded 6016 Aluminum Alloy/graphite Composites. Journal of Materials Science and Technology, 34:1580–1591. https://doi.org/10.1016/j.jmst.2018.03.004.

[34] Ahmed, M.M.Z., Ataya, S., El-Sayed Seleman, M.M., Ammar, H.R., Ahmed, E., 2017, Friction Stir Welding of Similar and Dissimilar AA7075 and AA5083. Journal of Materials Processing Technology, 242:77–91. https://doi.org/10.1016/j.jmatprotec.2016.11.024.

[35] Alzahrani, B., El-Sayed Seleman, M.M., Ahmed, M.M.Z., Elfishawy, E., Ahmed, A.M.Z., Touileb, K., Jouini, N., Habba, M.I.A., 2021, The Applicability of Die Cast A356 Alloy to Additive Friction Stir Deposition at Various Feeding Speeds. Materials, 14:6018. https://doi.org/10.3390/ma14206018.

[36] Singh, T.; Tiwari, S.K.; Shukla, D.K. Effect of nano-sized particles on grain structure and mechanical behavior of friction stir welded Al-nanocomposites. Proc. Inst. Mech. Eng. Part L J. Mater. Des. Appl. 2020, 234, 274–290, doi:(10.1177/1464420719885156).

[37] Das, D., Roy, D.K., Satpathy, M.P., Nanda, B.K., Nayak, R.K., 2019, Compressive, Impact and Flexural Behaviour of Al Based Metal Matrix Composites. Materials Today: Proceedings, 18:3080–3086. https://doi.org/10.1016/j.matpr.2019.07.180.
[38] Matli, P.R., Shakoor, R.A., Mohamed, A.M.A., 2018, Development of Metal Matrix Composites Using Microwave Sintering Technique. Sintering of Functional Materials. https://doi.org/10.5772/68081.
[39] Mohanavel, V., Ali, K.S.A., Prasath, S., Sathish, T., Ravichandran, M., 2020, Microstructural and Tribological Characteristics of AA6351/Si3N4 Composites Manufactured by Stir Casting. Journal of Materials Research and Technology, 9:14662–14672. https://doi.org/10.1016/j.jmrt.2020.09.128.
[40] Akbari, M.K., Baharvandi, H.R., Mirzaee, O., 2013, Nano-sized Aluminum Oxide Reinforced Commercial Casting A356 Alloy Matrix: Evaluation of Hardness, Wear Resistance and Compressive Strength Focusing on Particle Distribution in Aluminum Matrix. Composites Part B: Engineering, 52:262–268. https://doi.org/10.1016/j.compositesb.2013.04.038.
[41] Fouladi, S., Abbasi, M., 2017, The Effect of Friction Stir Vibration Welding Process on Characteristics of SiO2 Incorporated Joint. Journal of Materials Processing Technology, 243:23–30. https://doi.org/10.1016/j.jmatprotec.2016.12.005.
[42] Bahrami, M., Dehghani, K., Besharati Givi, M.K., 2014, A Novel Approach to Develop Aluminum Matrix Nano-composite Employing Friction Stir Welding Technique. Materials and Design, 53:217–225. https://doi.org/10.1016/j.matdes.2013.07.006.
[43] Rahmatian, B., Dehghani, K., Mirsalehi, S.E., 2020, Effect of Adding SiC Nanoparticles to Nugget Zone of Thick AA5083 Aluminium Alloy Joined by Using Double-sided Friction Stir Welding. Journal of Manufacturing Processes, 52:152–164. https://doi.org/10.1016/j.jmapro.2020.01.046.
[44] Barmouz, M., Besharati Givi, M.K., Seyfi, J., 2011, On the Role of Processing Parameters in Producing Cu/SiC Metal Matrix Composites via Friction Stir Processing: Investigating Microstructure, Microhardness, Wear and Tensile Behavior. Materials Characterization, 62:108–117. https://doi.org/10.1016/j.matchar.2010.11.005.
[45] Huang, Z., Yang, C., Qi, L., Allison, J.E., Misra, A., 2019, Dislocation Pile-ups at β1 Precipitate Interfaces in Mg-rare Earth (RE) Alloys. Materials Science and Engineering A, 742:278–286. https://doi.org/10.1016/j.msea.2018.10.104.
[46] Minak, G., Ceschini, L., Boromei, I., Ponte, M., 2010, Fatigue Properties of Friction Stir Welded Particulate Reinforced Aluminium Matrix Composites. International Journal of Fatigue, 32:218–226. https://doi.org/10.1016/j.ijfatigue.2009.02.018.
[47] Bharti, S., Ghetiya, N.D., Patel, K.M., 2021, A Review on Manufacturing the Surface Composites by Friction Stir Processing. Materials and Manufacturing Processes, 36:135–170. https://doi.org/10.1080/10426914.2020.1813897.
[48] Asadi, P., Faraji, G., Masoumi, A., Givi, M.K.B., 2011, Experimental Investigation of Magnesium-base Nanocomposite Produced by Friction Stir Processing: Effects of Particle Types and Number of Friction Stir Processing Passes. Metallurgical and Materials Transactions A: Physical Metallurgy and Materials Science, 42:2820–2832. https://doi.org/10.1007/s11661-011-0698-8.
[49] Naresh, P., Kumar, A., Kishore, M.K., 2017, Influence of Nano Reinforcement Volume Percentage on Fabrication of Surface Nanocomposite by FSP. Mater Sci Forum, 879:1369–1374. https://doi.org/10.4028/www.scientific.net/MSF.879.1369.